THE JOURNAL OF PHYSICAL CHEMISTRY LETTERS
A JOURNAL OF THE AMERICAN CHEMICAL SOCIETY

pubs.acs.org/JPCL

Letter

Characterizing Transient Protein−Protein Interactions by Trp-Cys Quenching and Computer Simulations

Lim Heo,[#] Kasun Gamage,[#] Gilberto Valdes-Garcia, Lisa J. Lapidus,* and Michael Feig*

Cite This: *J. Phys. Chem. Lett.* 2022, 13, 10175−10182

Read Online

ACCESS | Metrics & More | Article Recommendations | Supporting Information

ABSTRACT: Transient protein−protein interactions occur frequently under the crowded conditions encountered in biological environments. Tryptophan−cysteine quenching is introduced as an experimental approach with minimal labeling for characterizing such interactions between proteins due to its sensitivity to nano- to microsecond dynamics on subnanometer length scales. The experiments are paired with computational modeling at different resolutions including fully atomistic molecular dynamics simulations for interpretation of the experimental observables and to gain molecular-level insights. This approach is applied to model systems, villin variants and the drkN SH3 domain, in the presence of protein G crowders. It is demonstrated that Trp-Cys quenching experiments can differentiate between overall attractive and repulsive interactions between different proteins, and they can discern variations in interaction preferences at different protein surface locations. The close integration between experiment and simulations also provides an opportunity to evaluate different molecular force fields for the simulation of concentrated protein solutions.

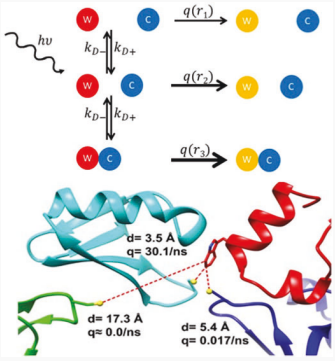

Biological cells are densely packed with proteins and other biomolecules at volume fractions of 20−40% in the aqueous phase.[1] Frequent encounters between diffusing proteins are unavoidable at such high concentrations, impacting protein diffusion, structure, and dynamics.[2−7] Varying propensities for aggregation and phase separation[8,9] add an additional dimension. A starting point for understanding crowding is the excluded-volume effect where diffusion is limited and where compact arrangements are favored for lack of free space.[10] Beyond this simplifying scenario, proteins may interact transiently to different degrees as a function of protein and concentration.[11−15] Dynamic clusters that persist on nanosecond to microsecond time scales can impact diffusion properties[16−19] or interfere with ligand binding events.[20] In fact, the slow-down in diffusion experienced by proteins in crowded environments may be primarily due to slower-diffusing transient clusters rather than increased solvent viscosity or reduced free space.[19,21] Experimental evidence has come primarily from the key observation that diffusion varies as a function of protein crowder species at the same volume fractions[22−24] and that rotational diffusion is slowed down as much as or more than translational diffusion,[12] a hallmark of interacting particles. Other approaches have explored transient interactions more directly in specific biological systems.[15,25−28] However, many questions remain about the determinants of transient interactions between two arbitrary proteins under highly concentrated conditions.

A direct characterization of the transient interactions between any pair of proteins via experiment is difficult as such interactions are short-lived and lack strong preferences for specific contacts. In this work, we introduce quenching of the tryptophan (Trp) triplet state by cysteine (Cys) as a new tool for examining the details of such interactions in concentrated solutions. Trp-Cys quenching has been used for many years for investigating intramolecular dynamics of disordered polypeptide chains.[29−34] A Trp residue within a folded protein is excited to a long-lived triplet state via the fluorescence singlet state. In the absence of quenchers, the lifetime of this state is ∼40 μs,[30] and it is much more efficiently quenched via electron transfer by Cys than by any other amino acid. Trp-Cys quenching is sensitive to microsecond dynamics over distances up to 10 Å, similar to typical bimolecular distances under physiological conditions,[5] when 1−3 water layers are separating macromolecules.[35] The Trp triplet in a concentrated solution may have a shorter lifetime than in dilute solutions, but it is still measurable so that contacts can be distinguished from close interactions. Trp-Cys quenching is thus well-suited for characterizing transient intermolecular encounters in concentrated solutions. A further advantage is that only natural amino acids are involved and additional labeling that may interfere with protein−protein interactions can be avoided. Moreover, because of the sensitivity to relatively short distances, the location of the probes on the protein surfaces

Received: September 2, 2022
Accepted: October 21, 2022
Published: October 24, 2022

provides spatial resolution that can be explored by mutating Trp or Cys residues. As Trp-Cys quenching decays in crowded conditions are difficult to interpret at the molecular level, computer simulations are needed to provide context. Molecular dynamics simulations of concentrated protein solutions in atomistic detail over microseconds are now possible,[36,37] and this work presents a close comparison between experiment and simulation, including an opportunity for validating the force field parameters used in the simulations. Once validated, the simulations can reveal additional information about protein−protein interactions at the molecular level. Together, this integrated experimental−computational approach provides direct, experiment-driven insights into transient protein interactions at elevated protein concentrations.

Experiments. Trp-Cys quenching experiments were carried out for villin or drkN SH3 probe molecules in the presence of protein G quenchers. Figure 1A shows the decay curves for the

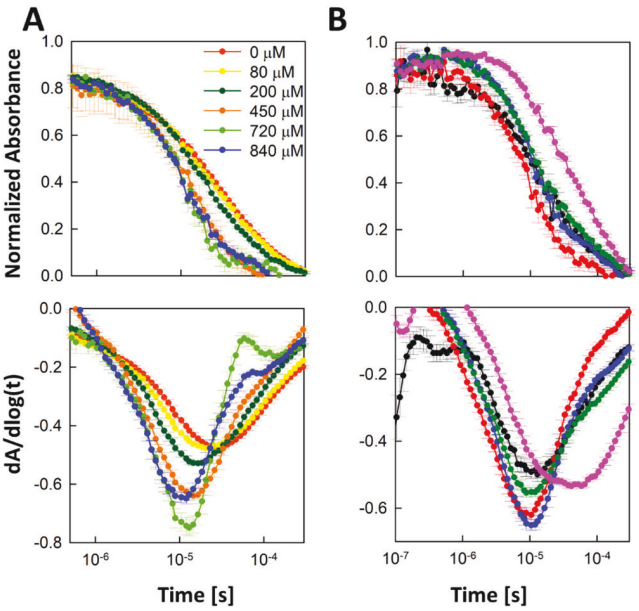

Figure 1. Experimental measurements of Trp triplet lifetime in villin variants and SH3 in the presence of protein G. Decays are shown as absorbance vs time (top) and as the derivatives of the decays vs log(t) calculated as the slope of a linear fit over a sliding window of 21 time points (bottom). (A) K33W at various concentrations of protein G. (B) Villin headpiece wild-type (black), V10W (red), K33W (blue), R15T+K30E (green), and SH3 (magenta). Curves were averaged from six independent measurements and normalized to 0.88 at 147 ns and to 0 at 369 μs. Error bars represent the standard deviation. Error bars in the derivatives represent the error of the fit.

K33W variant of villin at different concentrations of protein G along with their derivatives vs log(t). Without protein G, the decay curve reflects the unquenched lifetime of the Trp triplet state (40 μs). The slightly nonexponential decay is due to low-probability quenching by non-Cys amino acids within the folded structure.[30] Once protein G is added, decay occurs on shorter time scales due to Cys quenching. The resulting quenching rates in the presence of protein G still display nonexponential behavior as indicated by a broad, shallow minimum in the derivative of absorbance vs log(t). When the protein G concentration is increased, both the location of the minimum in time and the depth are affected. A shift to shorter times at higher concentrations results from more frequent protein−protein contacts. The depth changes as quenching shifts from slow but short-range intramolecular quenching by other amino acids in the villin to faster intermolecular quenching by cysteine from interacting protein G molecules.

The quenching curve for the SH3 domain is shifted significantly to longer times compared to the villin variants (Figure 1B and Table S1), indicating that interactions between different proteins can be distinguished. On the other hand, decay curves for different villin mutants at a fixed protein G concentration have varying depths of the derivative minimum with little shift in time. This suggests that differences in local interactions with respect to the Trp location (residue 24 in wild-type villin and the R15T+K30E mutant, and residues 10 and 33 in the V10W and K33W mutants, respectively) can be probed as well. Computational modeling results will explain the origin of the varying quenching curves below.

Modeling of Trp-Cys Quenching on 1D Potentials. A simple computer model was applied to interpret the experimental quenching curves. A 1D variable, the probe-quencher distance, was sampled stochastically via Monte Carlo (MC) simulation using different contact potentials (eq S1). Figure 2 shows quenching curves obtained with potentials that approximate Trp-Cys distance distributions extracted from atomistic simulations described below. The shape and characteristics of the decay curves are similar to the experiments. When potentials are varied with different contact minima depths and different kinetic barriers near the contact minimum (Figure 2A), the calculated quenching curves (Figure 2B) shift little in time but the derivative minimum varies in depth. The depth is most strongly correlated with the difference in probability between the contact minimum and large separation distances (calculated at 10 Å, Figure S1A). Weaker interactions with a shallower contact minimum result in a deeper derivative value, and *vice versa*, stronger interactions with a deeper contact minimum lead to shallower derivatives. The barrier height near the contact minimum, measured as the difference in energy at the peak vs the energy at 10 Å, has a smaller effect as higher barriers tend to shift the minimum down (Figure S1B). In addition, smaller barriers cause a slight shift to shorter times and with higher barriers to longer times (Figure S1D). If the potential is further modified by introducing long-range attraction or repulsion (Figure 2C), quenching curves shift to longer time scales with a deeper minimum in the case of repulsion; with long-range attraction the derivative minimum mainly shifts upward (Figure 2D). The shift to longer time scales in the case of repulsion is a result of less frequent contacts, whereas additional attraction does not significantly shift the time scale because most of the time is already spent in or near contact. The curves are also shifted in time when the system size is reduced (Figure S2). A reduced system size is a model for increased concentration, and the changes in the curves are similar as seen in the experiments at different protein G concentrations.

This analysis allows a first interpretation of the experimental data. The shift to longer time scales for SH3 vs villin, at the same concentrations, reflects long-range repulsion between SH3 and protein G relative to villin and protein G. This may be expected as both SH3 (−6) and protein G (−5) have net negative charges, whereas villin has a net positive (+2) or slightly negative (−1) charge for the double mutant. On the other hand, the observed differences between villin variants appear to stem from different contact potentials near villin

https://doi.org/10.1021/acs.jpclett.2c02723
J. Phys. Chem. Lett. 2022, 13, 10175−10182

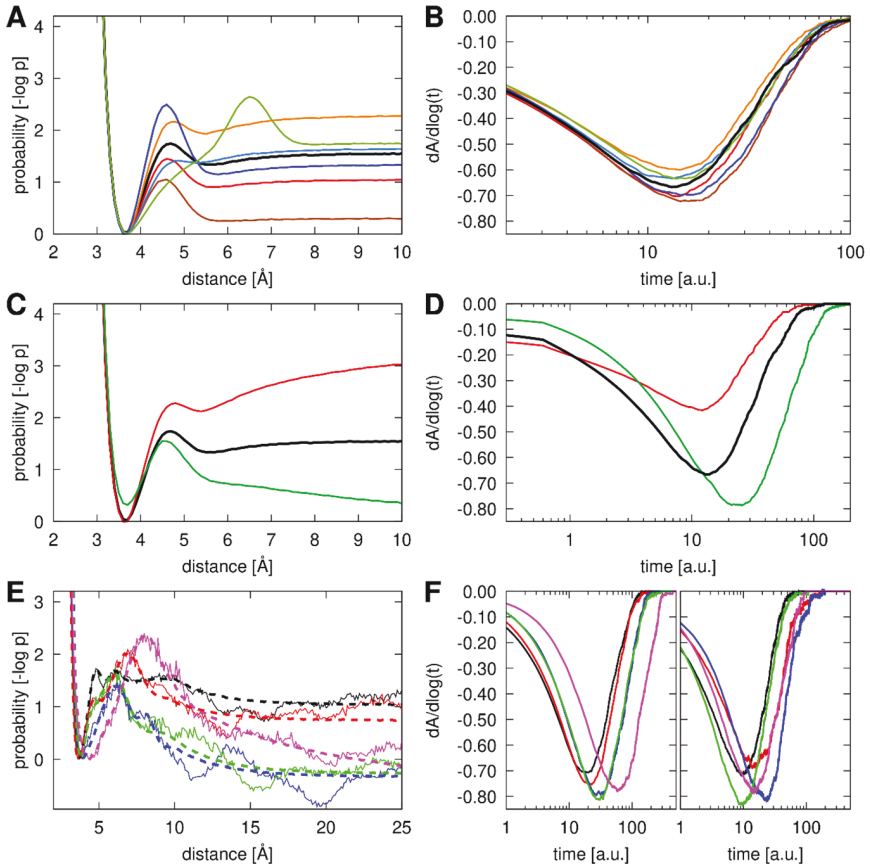

Figure 2. Computational modeling of Trp-Cys quenching via 1D potentials. Probability distribution functions are shown on the left (A, C, E), and derivatives of the calculated quenching curves are shown on the right (B, D, F). The reference distribution in black in parts A–D is based on the contact probability extracted from atomistic simulations for the wild-type villin structure (E). Variations in the potential near the contact minimum are shown in parts A and C. Variations in long-range attraction ($d = -1$ in eq S1, red) or repulsion ($d = 1$ in eq S1, green) are shown in C and D. Trp-Cys contact probability functions from atomistic simulations are shown in E (solid lines) along with fitted 1D potentials (dashed lines). Atomistic probabilities are for minimum villin-protein G Trp-Cys distances. Distances are limited to 25 Å since there is almost always a protein G molecule sufficiently close for minimum distances to be less than 30 Å due to crowding. Derivatives on the left in part F were obtained with uniform Monte Carlo sampling. Derivatives on the right in part F resulted from sampling with diffusion-matched, distance-dependent step sizes (see Supporting Information). Colors in parts E and F reflect different probes: villin wild-type (black), villin V10W (red), villin K33W (blue), villin R15T+K30E (green), SH3 (magenta).

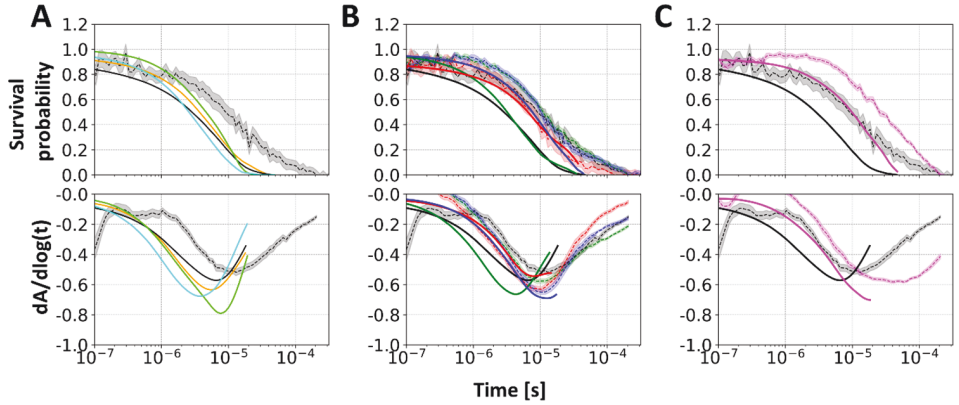

Figure 3. Comparison of survival probability decays between experimental measurements and simulated data. The probability and its derivative against log-time are shown at top and bottom of each panel, respectively. Derivative values were obtained from a linear fit of probabilities against log-time with a window size of 21. Experimental values shown as solid lines with transparent shades for standard errors were adjusted to match the simulated data at 100–500 ns since the initial decay varies in the simulations and experiments are not sensitive to quenching during the initial 100 ns after excitation. (A) Results for wild-type villin obtained using different force fields c36 (orange), c36+water (lime), c36m (black), and c36mw (cyan). (B) Results with c36m for wild-type villin (black), V10W (red), K33W (blue), and the R15T+K30E double mutant (green). (C) Results with c36m for wild-type villin (black) and SH3 (magenta).

https://doi.org/10.1021/acs.jpclett.2c02723
J. Phys. Chem. Lett. 2022, 13, 10175–10182

residue 24 (wild-type and R15T+K30E), near residue 10 (V10W mutant), or near residue 33 (K33W mutant), since the derivative minima are deeper for the V10W and K33W single mutants than for the wild-type and double mutant. There is also a difference between the wild-type and double mutant with the deeper minimum for the double mutant suggesting weaker interactions, presumably due to a more negative charge compared to the wild-type.

Atomistic Simulations of Trp-Cys Quenching. To further interpret the experimental observations at the molecular level, we applied μs-scale molecular dynamics (MD) simulations. The simulations sample the diffusion and interactions between the proteins in the same systems that were studied experimentally. The survival probabilities of the triplet state of Trp were calculated from the simulation according to eq 1 based on the distance between Trp and Cys residues, including time-scale corrections (see methods section). They are compared with the experimental results in Figure 3. For wild-type villin, we considered four CHARMM force field variants c36,[38] c36+water,[16] c36m,[39] and c36mw[39] (Figure 3A). All force fields resulted in somewhat faster decay curves compared to experiment. That is discussed further below. Depending on the force field, the minimum depth in the derivative of the survival probability function varies. The deepest minimum is found for c36+water, followed by c36mw,[39] both of which decrease protein−protein interactions by scaling water interactions (Figure S3). Shallower minima are found for c36m[39] and c36[38] where protein interactions are stronger according to larger and longer-lived transient clusters (Figure S4). C36 and c36m perform similarly, but the agreement with the experimental data is somewhat better for c36m. c36m has also been found to perform well in other contexts.[39−41] Therefore, we subsequently focus on simulations using c36m.

The simulations capture many of the features seen in the experimental quenching curves (Figure 3B). The double mutant, R15T+K30E, has a deeper minimum in the derivative than the wild-type, presumably due to weaker local interactions. The K33W mutant shows weaker interactions than V10W as in the experiment. For both single mutants, the derivatives of the survival probabilities are in excellent agreement with experiment, but the minima of the wild-type and double mutant are both shifted downward and to shorter times compared to experiment. Comparing wild-type villin with SH3, the simulations show a similar shift to longer times and with a deeper minimum for SH3 as in experiment (Figure 3C).

The shifts in time scale are not explained by differences in translational diffusion (Table S2). Diffusion is similar for all villin variants and SH3, even although SH3 is heavier than villin (6811.5 vs 4214.9 g/mol), essentially because of less cluster formation with SH3 (Figure S5). To further understand these results, we turn again to the 1D model introduced above. Trp-Cys distance probabilities extracted from the atomistic simulations have a clear contact minimum around 3.5−4 Å for villin and at 4−5 Å for SH3, followed by a barrier at varying locations at 4.5−8 Å (Figure 2E). There is also a longer-range decline of distance probabilities with a plateau for villin mutants reached at 15 Å, whereas the decline continues to longer distances for SH3. A depletion beyond 10 Å is generally expected as protein G favors interactions with villin due to crowding but may interact in many arrangements that do not place protein G's C10 near the villin Trp. MC sampling was carried out on 1D potentials fitted to reproduce the atomistic contact probabilities (Figure 2E,F). When only the short-range potential (<10 Å) is considered, quenching occurs on similar time scales and the derivative minima are ordered mostly as in the experiment (i.e., the double mutant is lower than wild-type villin, and V10W and K33W are lower than the wild-type) (Figure S6). When the long-range decay of the Trp-Cys contact probability is added, the villin variants shift slightly in time while maintaining their order, whereas the decay for SH3 shifts more significantly to slower times because of longer-range repulsion, again qualitatively similar to experiment (Figure 2E,F). This analysis explains the experimental data directly from distance contact probabilities extracted from the atomistic simulations.

We now turn to the shift to shorter times in the quenching curves for wild-type villin and the double mutant in the atomistic simulations. We found that although contact potentials are similar, diffusion in the Trp-Cys distance differs significantly (Figure S7). At a distance around 10 Å, diffusion is about twice for wild-type villin and about 5-fold for the double mutant and SH3 compared to diffusion in the V10W and K33W mutants at that distance. MC sampling with a fixed maximum step size does not reproduce such differences in kinetics (Figure S7B). However, by introducing variable MC step sizes for different systems (see methods section), diffusion kinetics similar to the atomistic simulations can be obtained via MC sampling (Figure S7D). Once the 1D potentials were resampled with the modified pseudokinetics, quenching curves for wild-type villin, the double mutant, and SH3 were shifted to shorter time scales relative to V10W and K33W as in the atomistic simulations (Figure 2F). The depth of the minima also changed slightly, with the wild-type curves now lower than V10W as in the atomistic simulations indicating that altered kinetics also affect the quenching curve derivative minima.

This leaves the question why the Trp-Cys distances fluctuate more rapidly with respect to Trp at the villin 24 position (probed by the wild-type and double mutant) vs Trp at the 10 and 33 positions in the simulations but not in the experiment. As stated above, overall protein diffusion is not significantly different between the villin variants. Trp-Cys contact lifetimes based on contact correlation analysis are also similar between wild-type and the single mutants (Figure S8). However, conformational fluctuations of the Trp residue itself vary depending on where it is located in the villin structure (Figure S9). With or without protein G, Trp (or Tyr when substituted in V10W and K33W) is more dynamic at the 24 position vs Trp at the 10 and 33 positions. The differences become significant at time scales beyond about 10 ns when protein G is present (Figure S9). Since the systems studied via simulation are more concentrated than in experiment, villin−protein G interactions persist long enough for Trp fluctuations to affect the quenching rates. More specifically, it appears that the faster quenching rates for wild-type villin and the double mutant relative to V10W and K33W result from long associations between villin and protein G in arrangements such as the ones shown in Figure S10 and Movie S1 where the dynamics in the Trp-Cys distance is due in part to fluctuations of W24. For comparison, Movie S2 shows quenching at V10W where the Trp is more rigid. To further test this idea, we calculated hypothetical quenching curves relative to the residue at position 24 (Tyr for V10W and K33W) based on the V10W and K33W simulations. The resulting quenching curves are shifted also for V10W and K33W (Figure S11). Therefore, we

https://doi.org/10.1021/acs.jpclett.2c02723
J. Phys. Chem. Lett. 2022, 13, 10175−10182

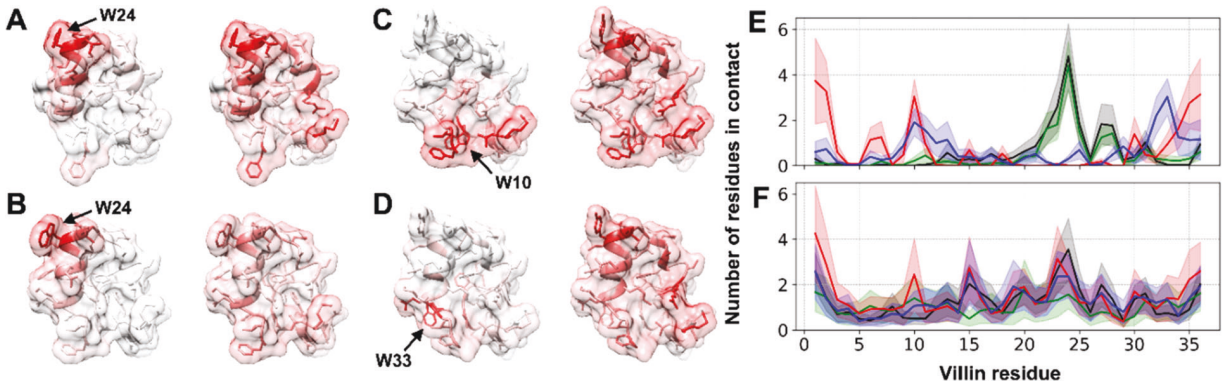

Figure 4. Residuewise contacts between protein G and villin variants, projected onto the villin surface (A–D) and as a function of villin residue index (E, F). Surface projections are shown for Trp-Cys quenching contact (left) and for all contact positions (right) for wild-type villin (A), the R15T+K30E mutant (B), the V10W mutant (C), and the K33W mutant (D). The location of the Trp residue is indicated by arrows. Contacts per frame vs residue index are shown at the time of quenching contact (E) and at any time of contact (F) with different variants colored as in Figure 1. Shaded areas indicate standard errors. Contacts were defined by residue pairs whose interatomic distances were closer than 5 Å.

conclude that the dynamics at the 24 position of villin is determining the faster kinetics in the simulations instead of other differences due to the V10W and K33W mutations.

Based on the simulations, we find that overall villin–protein G interaction preferences are similar for the three variants (Figure 4F). Interactions between protein G and villin residue 24 are slightly preferred over interactions near villin residue 10 or 33 (Figures 4F and S12), but strong preferences for the vicinity of residue 24 only emerge when focusing specifically on quenching interactions (Figure 4E), meaning when the vicinity of protein G C10 is interacting with villin. In more detail, it appears that quenching near residue 24 is highly specific to the immediate vicinity of residue 24 (Figure 4A,B,E), whereas quenching near V10W and K33W is broader (Figure 4C,D,E and Figure S13). This may be expected since the surface near 10 and 33 is flatter compared to the 24 site pointing into solvent at the tip of the villin structure. From the perspective of protein G, the vicinity of C10 is highly preferred for interactions with villin but there is little difference when interacting with different villin variants (Figure S14). This suggests that the Trp-Cys quenching experiments are a highly sensitive tool for mapping out residue-specific transient interactions involving both the probe and quencher and that the integration with simulations can provide additional details.

Trp-Cys quenching is a highly sensitive tool to investigate close-range interactions on the time scales in which transient interactions occur under concentrated conditions. The comparison between villin and SH3 shows that Trp-Cys quenching can distinguish interaction strengths between different proteins, and mutants of villin show relative preferences over the surface of the protein. Note that these results were validated despite the relatively low concentration of protein G in the experiments compared to the simulations. Moving the location of the Trp to additional points on the villin or SH3 surface or moving the Cys to other locations on the protein G surface should provide a more complete map of interaction preferences. A key part of this work was the interpretation of the experimental data by computational modeling and atomistic simulations. We show that we can come to similar conclusions either based on experiment, interpreted via the 1D model, or based on simulations, after appropriate time scale corrections. This validates the simulations, but more importantly it confirms the interpretation of the experiments via the 1D modeling.

The results suggest a number of ways to move forward with this technique. On the experimental side, a comparison of decay curves for different mutants of any two proteins will highlight the relative strength of bimolecular interactions. The need for Trp and Cys residues on the protein surfaces places some limitations on the systems that can be studied, but the main requirements are that only one protein has at most a small number of Trp residues on the surface and that there are no Cys residues on the probe protein near the Trp to avoid self-quenching. Analysis of quenching curves with a single Trp residue is more straightfoward, but quenching with multiple Trp residues may be deconvoluted via modeling. Since natural abundance of Trp is low, the requirements can be easily satisfied for many proteins either with wild-type sequences or via a small number of mutations. Protein solubility, especially at concentrations approaching biological cellular conditions, is a significant problem for *in vitro* experiments. We could not reach higher concentrations for the systems studied here, but we expect that this will be possible with alternate constructs, for different systems, or by using condensates. Our previous work on condensation of folded proteins and RNA shows that such condensates are possible.[42] There is otherwise no fundamental reason why Trp-Cys quenching could not be applied at higher concentrations. To support this point, we calculated unscaled quenching curves from simulations at 33 and 66 g/L, more than 10 times higher than in the experiments (Figure S15). According to the simulations, the majority of the absorbance decay occurs between 100 ns and 1 μs, well above the instrument limit of around 20 ns. However, even if higher concentrations cannot be reached in the experiments, the present study demonstrates how the combination with simulations allows extrapolation to higher concentrations.

On the computational side, the 1D model is an inexpensive way to visualize the potentials of mean force between proteins. Hypothetical potentials can be convolved with the quenching mechanism to produce decay curves that may be compared with experiments. It remains to be explored whether this can be taken a step further by developing a protocol in which an interaction potential is extracted directly from experimental data under certain assumptions, such as fixed concentrations

https://doi.org/10.1021/acs.jpclett.2c02723
J. Phys. Chem. Lett. 2022, 13, 10175–10182

and with a focus on relative differences between proteins in comparison to a known reference.

Atomistic simulations provide a more complete picture, such as the role of side chain fluctuations in accelerating quenching rates under crowded conditions. While we have compared different force fields for the systems studied here, additional experiments on a wider site of systems will allow a more comprehensive force field assessment in future work. In another direction, the present work may also facilitate the development and assessment of predictive CG models to avoid the large computational costs of atomistic simulations. The degree to which various types of simulation, modeling, and experiment are deployed to understand protein−protein interactions will depend on the questions that need to be addressed.

EXPERIMENTAL AND COMPUTATIONAL METHODS

Systems. Sequence variations of the HP35 fragment of the villin headpiece (see Table S3) and the T22G mutant of the drkN SH3 domain, each with one Trp, were studied in the presence of the B1 domain of protein G, mutated to contain one Cys (K10C) and no Trp (W43Y).

Experiments. Villin and SH3 concentrations were held constant at 30 μM. Concentrations of protein G were varied up to 0.84 mM. The decay of the Trp triplet state was measured with a two-laser pump−probe setup: a 10 ns pulse at 289 nm excites the triplet state, while a continuous wave laser at 450 nm probes the population of the triplet state by transient absorption. A background due to additional excitation of four tyrosines in the concentrated protein G was subtracted (Figure S16).

In Trp-Cys quenching, the Trp triplet decays exponentially with the quencher distance as

$$q(r) = k_0 \exp(-\beta(r - a)) \tag{1}$$

with a = 3.5 Å (distance of closest approach), $k_0 = 4.2 \times 10^9$ s^{-1} (decay rate at a), and β = 4 $Å^{-1}$ (decay constant). With the large value of β, decay rates remain significant up to distances of about a + 5 Å. Interactions within this range or diffusion in and out of close interactions on time scales shorter than the triplet state lifetime, i.e., <40 μs, results in nonexponential decay.

Monte Carlo Sampling of 1D Potentials. 1D potentials were constructed with strong repulsion at close distances and weak attraction at a contact distance. Additional Gaussian functions were used to model kinetic barriers and kinetic traps at different distances (Figure 2). The potential was sampled via MC sampling to create diffusive pseudodynamics without a meaningful time scale, but desired diffusion kinetics can be imposed by varying the MC step size.

Atomistic Simulations. MD simulations in atomistic detail were carried out for the experimentally studied systems but at 5-fold higher concentrations because of computational cost. Multiple simulations on μs time scales were carried out with different force fields (Table S4). Simulation results were adjusted in time-scale to compare with the experimental results. Differences in protein concentrations were accounted for by extrapolation guided by coarse-grained MD simulations (Figure S17). Additional time-scale corrections were applied to correct for underestimated solvent viscosity and artifacts due to periodic boundaries estimated based on protein diffusion calculated from mean square displacements (Figure S18 and Table S2).

Calculation of Triplet State Survival Probability. From sampled probe-quencher distance−time series, survival probability curves were calculated from eq 2 using the quenching function in eq 1 for the distances sampled via MC or MD.

$$S_{\text{quenching}}(t) = \left\langle \exp\left(-\int_0^t q(t')\,dt'\right)\right\rangle = \frac{1}{t_{\max} - t}\sum_0^{t_{\max}-t} \exp\left(-\int_0^t q(t')\,dt'\right) \tag{2}$$

The triplet-to-singlet transition due to autobleaching was considered via eq 3 with an autobleaching rate constant (k_0) of 2.3×10^{-5}/ns.[30]

$$S(t) = S_{\text{quenching}}(t)\, e^{-k_0 t} \tag{3}$$

ASSOCIATED CONTENT

Supporting Information

The Supporting Information is available free of charge at https://pubs.acs.org/doi/10.1021/acs.jpclett.2c02723.

Details on sample preparation, experments, and simulations; Figures S1−S27; Tables S1−S7; captions for Movies S1 and S2; and additional references (PDF)

Movie S1 showing Trp-Cys contact formation between wild-type villin and protein G (MP4)

Movie S2 showing Trp-Cys contact formation between villin V10W and protein G (MP4)

Transparent Peer Review report available (PDF)

AUTHOR INFORMATION

Corresponding Authors

Lisa J. Lapidus − *Department of Physics and Astronomy, Michigan State University, East Lansing, Michigan 48824, United States;* orcid.org/0000-0003-3136-2680; Phone: +1-517-884-5656; Email: lapidus@msu.edu

Michael Feig − *Department of Biochemistry and Molecular Biology, Michigan State University, East Lansing, Michigan 48824, United States;* orcid.org/0000-0001-9380-6422; Phone: +1-517-432-7439; Email: mfeiglab@gmail.com

Authors

Lim Heo − *Department of Biochemistry and Molecular Biology, Michigan State University, East Lansing, Michigan 48824, United States;* orcid.org/0000-0002-3153-2363

Kasun Gamage − *Department of Physics and Astronomy, Michigan State University, East Lansing, Michigan 48824, United States*

Gilberto Valdes-Garcia − *Department of Biochemistry and Molecular Biology, Michigan State University, East Lansing, Michigan 48824, United States*

Complete contact information is available at: https://pubs.acs.org/10.1021/acs.jpclett.2c02723

Author Contributions

#L.H. and K.G. are co-first authors.

Notes

The authors declare no competing financial interest.

A Jupyter notebook illustrating the Monte Carlo simulation of 1D potentials to reproduce Trp-Cys quenching experiments is available on GitHub: https://github.com/feiglab/mc-trpcys.

■ ACKNOWLEDGMENTS

Funding was provided by the National Science Foundation Grants MCB 1817307 and by the National Institute of Health (NIGMS) Grant R35 GM126948. Computer time was used on the Anton2 special-purpose supercomputer at the Pittsburgh Supercomputing Center (Grant PSCA18053P).

■ REFERENCES

(1) Ellis, R. J. Macromolecular crowding: an important but neglected aspect of the intracellular environment. *Curr. Opin. Struct. Biol.* **2001**, *11*, 114−119.
(2) Danielsson, J.; Oliveberg, M. Comparing protein behaviour *in vitro* and *in vivo*, what does the data really tell us? *Curr. Opin. Struct. Biol.* **2017**, *42*, 129−135.
(3) Rivas, G.; Minton, A. P. Macromolecular crowding *in vitro*, *in vivo*, and in between. *Trends Biochem. Sci.* **2016**, *41*, 970−981.
(4) Zimmerman, S. B.; Minton, A. P. Macromolecular crowding - biochemical, biophysical, and physiological consequences. *Annu. Rev. Biophys. Biomol. Struct.* **1993**, *22*, 27−65.
(5) Yu, I.; Mori, T.; Ando, T.; Harada, R.; Jung, J.; Sugita, Y.; Feig, M. Biomolecular interactions modulate macromolecular structure and dynamics in atomistic model of a bacterial cytoplasm. *eLife* **2016**, *5*, e19274.
(6) Monteith, W. B.; Cohen, R. D.; Smith, A. E.; Guzman-Cisneros, E.; Pielak, G. J. Quinary structure modulates protein stability in cells. *Proc. Natl. Acad. Sci. U.S.A.* **2015**, *112*, 1739−1742.
(7) Wirth, A. J.; Gruebele, M. Quinary protein structure and the consequences of crowding in living cells: leaving the test-tube behind. *BioEssays* **2013**, *35*, 984−993.
(8) Alberti, S.; Gladfelter, A.; Mittag, T. Considerations and challenges in studying liquid-liquid phase separation and biomolecular condensates. *Cell* **2019**, *176*, 419−434.
(9) Boeynaems, S.; Alberti, S.; Fawzi, N. L.; Mittag, T.; Polymenidou, M.; Rousseau, F.; Schymkowitz, J.; Shorter, J.; Wolozin, B.; Van den Bosch, L.; et al. Protein phase separation: a new phase in cell biology. *Trends Cell Biol.* **2018**, *28*, 420−435.
(10) Minton, A. P. Excluded volume as a determinant of macromolecular structure and reactivity. *Biopolymers* **1981**, *20*, 2093−2120.
(11) Braun, M. K.; Grimaldo, M.; Roosen-Runge, F.; Hoffmann, I.; Czakkel, O.; Sztucki, M.; Zhang, F. J.; Schreiber, F.; Seydel, T. Crowding-controlled cluster size in concentrated aqueous protein solutions: structure, self- and collective diffusion. *J. Phys. Chem. Lett.* **2017**, *8*, 2590−2596.
(12) Roos, M.; Ott, M.; Hofmann, M.; Link, S.; Rössler, E.; Balbach, J.; Krushelnitsky, A.; Saalwächter, K. Coupling and decoupling of rotational and translational diffusion of proteins under crowding conditions. *J. Am. Chem. Soc.* **2016**, *138*, 10365−10372.
(13) Perkins, J. R.; Diboun, I.; Dessailly, B. H.; Lees, J. G.; Orengo, C. Transient protein-protein interactions: structural, functional, and network properties. *Structure* **2010**, *18*, 1233−1243.
(14) Rickard, M. M.; Zhang, Y.; Gruebele, M.; Pogorelov, T. V. In-cell protein−protein contacts: transient interactions in the crowd. *J. Phys. Chem. Lett.* **2019**, *10*, 5667−5673.
(15) Wang, Q. H.; Zhuravleva, A.; Gierasch, L. M. Exploring weak, transient protein-protein interactions in crowded *in vivo* environments by in-cell nuclear magnetic resonance spectroscopy. *Biochemistry* **2011**, *50*, 9225−9236.
(16) Nawrocki, G.; Wang, P.-h.; Yu, I.; Sugita, Y.; Feig, M. Slow-down in diffusion in crowded protein solutions correlates with transient cluster formation. *J. Phys. Chem. B* **2017**, *121*, 11072−11084.
(17) von Bülow, S.; Siggel, M.; Linke, M.; Hummer, G. Dynamic cluster formation determines viscosity and diffusion in dense protein solutions. *Proc. Natl. Acad. Sci. U.S.A.* **2019**, *116*, 9843.
(18) Nawrocki, G.; Im, W.; Sugita, Y.; Feig, M. Clustering and dynamics of crowded proteins near membranes and their influence on membrane bending. *Proc. Natl. Acad. Sci. U.S.A.* **2019**, *116*, 24562−24567.
(19) Nawrocki, G.; Karaboga, A.; Sugita, Y.; Feig, M. Effect of protein−protein interactions and solvent viscosity on the rotational diffusion of proteins in crowded environments. *Phys. Chem. Chem. Phys.* **2019**, *21*, 876−883.
(20) Kasahara, K.; Re, S.; Nawrocki, G.; Oshima, H.; Mishima-Tsumagari, C.; Miyata-Yabuki, Y.; Kukimoto-Niino, M.; Yu, I.; Shirouzu, M.; Feig, M.; Sugita, Y. Reduced efficacy of a Src kinase inhibitor in crowded protein solution. *Nat. Commun.* **2021**, *12*, 4099.
(21) Rothe, M.; Gruber, T.; Gröger, S.; Balbach, J.; Saalwächter, K.; Roos, M. Transient binding accounts for apparent violation of the generalized Stokes-Einstein relation in crowded protein solutions. *Phys. Chem. Chem. Phys.* **2016**, *18*, 18006−18014.
(22) Stadmiller, S. S.; Aguilar, J. S.; Parnham, S.; Pielak, G. J. Protein−peptide binding energetics under crowded conditions. *J. Phys. Chem. B* **2020**, *124*, 9297−9309.
(23) Wang, Y.; Li, C.; Pielak, G. J. Effects of proteins on protein diffusion. *J. Am. Chem. Soc.* **2010**, *132*, 9392−9397.
(24) Feig, M.; Sugita, Y. Variable interactions between protein crowders and biomolecular solutes are important in understanding cellular crowding. *J. Phys. Chem. B* **2012**, *116*, 599−605.
(25) Li, Y.-C.; Rodewald, L. W.; Hoppmann, C.; Wong, E. T.; Lebreton, S.; Safar, P.; Patek, M.; Wang, L.; Wertman, K. F.; Wahl, G. M. A versatile platform to analyze low-affinity and transient protein-protein interactions in living cells in real time. *Cell Rep.* **2014**, *9*, 1946−1958.
(26) Bartholow, T. G.; Sztain, T.; Patel, A.; Lee, D. J.; Young, M. A.; Abagyan, R.; Burkart, M. D. Elucidation of transient protein-protein interactions within carrier protein-dependent biosynthesis. *Commun. Biol.* **2021**, *4*, 340.
(27) Morell, M.; Espargaró, A.; Avilés, F. X.; Ventura, S. Detection of transient protein−protein interactions by bimolecular fluorescence complementation: The Abl-SH3 case. *Proteomics* **2007**, *7*, 1023−1036.
(28) Darie, C. C.; Deinhardt, K.; Zhang, G.; Cardasis, H. S.; Chao, M. V.; Neubert, T. A. Identifying transient protein−protein interactions in EphB2 signaling by blue native PAGE and mass spectrometry. *Proteomics* **2011**, *11*, 4514−4528.
(29) Lapidus, L. J.; Eaton, W. A.; Hofrichter, J. Dynamics of intramolecular contact formation in polypeptides: distance dependence of quenching rates in a room-temperature glass. *Phys. Rev. Lett.* **2001**, *87*, 258101.
(30) Lapidus, L. J.; Eaton, W. A.; Hofrichter, J. Measuring the rate of intramolecular contact formation in polypeptides. *Proc. Natl. Acad. Sci. U.S.A.* **2000**, *97*, 7220−7225.
(31) Woodard, J.; Srivastava, K. R.; Rahamim, G.; Grupi, A.; Hogan, S.; Witalka, D. J.; Nawrocki, G.; Haas, E.; Feig, M.; Lapidus, L. J. Intramolecular diffusion in α-synuclein: it depends on how you measure it. *Biophys. J.* **2018**, *115*, 1190−1199.
(32) Waldauer, S. A.; Bakajin, O.; Lapidus, L. J. Extremely slow intramolecular diffusion in unfolded protein L. *Proc. Natl. Acad. Sci. U.S.A.* **2010**, *107*, 13713.
(33) Lapidus, L. J.; Eaton, W. A.; Hofrichter, J. Measuring dynamic flexibility of the coil state of a helix-forming peptide. *J. Mol. Biol.* **2002**, *319*, 19−25.
(34) Singh, V. R.; Lapidus, L. J. The intrinsic stiffness of polyglutamine peptides. *J. Phys. Chem. B* **2008**, *112*, 13172−13176.
(35) Harada, R.; Sugita, Y.; Feig, M. Protein crowding affects hydration structure and dynamics. *J. Am. Chem. Soc.* **2012**, *134*, 4842−4849.
(36) Heo, L.; Sugita, Y.; Feig, M. Protein assembly and crowding simulations. *Curr. Opin. Struct. Biol.* **2022**, *73*, 102340.
(37) Feig, M.; Sugita, Y. Whole-cell models and simulations in molecular detail. *Annu. Rev. Cell Dev. Biol.* **2019**, *35*, 191−211.
(38) Best, R. B.; Zhu, X.; Shim, J.; Lopes, P.; Mittal, J.; Feig, M.; MacKerell, A. D., Jr Optimization of the additive CHARMM all-atom

protein force field targeting improved sampling of the backbone ϕ, ψ and side-chain χ_1 and χ_2 dihedral angles. *J. Chem. Theory Comput.* **2012**, *8*, 3257−3273.
(39) Huang, J.; Rauscher, S.; Nawrocki, G.; Ran, T.; Feig, M.; de Groot, B. L.; Grubmüller, H.; MacKerell, A. D., Jr. CHARMM36m: an improved force field for folded and intrinsically disordered proteins. *Nat. Methods* **2017**, *14*, 71−73.
(40) Samantray, S.; Yin, F.; Kav, B.; Strodel, B. Different force fields give rise to different amyloid aggregation pathways in molecular dynamics simulations. *J. Chem. Inf. Model.* **2020**, *60*, 6462−6475.
(41) Nerenberg, P. S.; Head-Gordon, T. New developments in force fields for biomolecular simulations. *Curr. Opin. Struct. Biol.* **2018**, *49*, 129−138.
(42) Dutagaci, B.; Nawrocki, G.; Goodluck, J.; Ashkarran, A. A.; Hoogstraten, C. G.; Lapidus, L. J.; Feig, M. Charge-driven condensation of RNA and proteins suggests broad role of phase separation in cytoplasmic environments. *eLife* **2021**, *10*, e64004.

https://doi.org/10.1021/acs.jpclett.2c02723
J. Phys. Chem. Lett. 2022, 13, 10175−10182